Asian Journal of Chemistry; Vol. 25, No. 14 (2013), 8082-8086

ASIAN JOURNAL OF CHEMISTRY

http://dx.doi.org/10.14233/ajchem.2013.15120

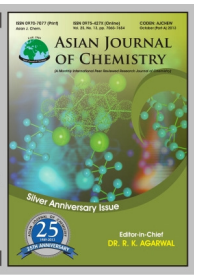

Synthesis of Co-Cu/La_2O_3 Pervoskites for Hydrogenation of CO

NGUYEN TIEN THAO

Faculty of Chemistry, VNU University of Science, Vietnam National University, 19 Le Thanh Tong ST, Hanoi, Vietnam

Corresponding author: Fax: +84 4 38241140; Tel: +84 4 39331605; E-mail: ntthao@vnu.edu.vn

(*Received*: 9 January 2013; *Accepted*: 1 August 2013) AJC-13878

Two families of $LaCo_{1-x}Cu_xO_{3-\delta}$ perovskites were synthesized by the conventional citrated complex and milling method. An introduction of copper in perovskite lattice gives rise to a slightly distorted structure of $LaCoO_3$ and influences the perovskite reducibility. Temperature programmed reduction analysis indicates the reduction of Co^{3+}, Cu^{2+} respectively to Co^{2+} and metallic copper over conventional samples at 310-580 ºC while that on ground perovskites in the temperature range of 320-610 ºC. The reduction of $La(Co,Cu)O_3$ yields a finely dispersed bimetal on a La_2O_3 support. The proximity of Co^{3+} and Cu^{2+} in perovskite structure leads to the formation of cobalt-copper alloy after reduction, which acts as active sites for the hydrogenation of CO into alcohols and hydrocarbon products.

Key Words: Perovskite, $LaCoCuO_3$, Co-Cu dispersion, Higher alcohol, Syngas, Alloy.

INTRODUCTION

Perovskite-type mixed oxides (ABO_3) in which the A and B sites are filled by rare-earth (Ln) and transition metals are well known catalysts and/or precursors for several oxidation/reduction reactions[1-3]. The ideal perovskite structure is cubic with space group Pm_3m-O_h^4.

However, distortions owing to ionic size requirements of the lattice framework give rise to the structure to be modified, usually by tilting or twisting of the octahedra[1,4]. Such distortions have changed in framework parameters and the unit cell volume and also lead to accommodate reduction in symmetry[5,6]. The perovskite framework is quite flexible of changes in the radii of A and B cations[5,6]. This allows a great flexibility in mixing cation of A and B sites to obtain several desired physical amd chemical properties[2,5-8]. Accordingly, perovskites have offered various interesting features as precursors for supported metal catalysts. Nevertheless, the catalytic activity of perovskite compounds is controlled mostly by the B-site metal while the effect of La ion sites is meager[2,3]. Thus, the reduction under controlled reduction conditions of $LnBO_3$ (B = Ni, Co, Fe…) can produce a well dispersed transition metal B on Ln_2O_3 support[2,7,9]. The reduced perovskites were used as catalysts for water gas shift reaction[2], partial oxidation of methane[10], reforming of methane[11], alkene hydrogenation[12] and Fischer-Tropsch synthesis[3]. Nevertheless, the catalytic activity of these perovskite-type oxides as catalysts/precursors is strongly dependant on the preparation process and their texture as well. This article reports the catalytic properties of two $La(Co,Cu)O_3$ perovskites prepared by two different methods and the use of their reduced perovskites in the hydrogenation of carbon monoxide.

EXPERIMENTAL

Preparation of $LaCoCuO_{3-\delta}$ perovskites: A family of conventional perovskites, $LaCo_{1-x}Cu_xO_{3-\delta}$ ($0 \le x \le 0.6$) named as CT1-CT5, was prepared by citrate method: a stoichiometric amount of lanthanum, cobalt and copper nitrates was added into the distilled water while slowly heating the mixture in a hot plate. After obtaining the clear transparent solution, a mole of citric acid corresponding to every mole of the metal atom was added to the dark pink transparent solution. The resulting solution was evaporated at 383 K overnight to yield an amorphous solid precursor. The precursors were then calcined at desired temperature for 6 h (2 ºC/min) under air.

Another series of $La(Co,Cu)O_3$ perovskite-type mixed oxides was synthesized by milling directly from their oxides. A mixture of lanthanum, copper and cobalt oxide (99 %, Aldrich) in stoichiometric proportions was blended together in a sealed 50 mL-hardened-steel crucible having three hardened steel 11 mm-diameter balls. Milling was performed at 1000 rpm for 8 h prior to a second milling step. After that, the resulting powder was mixed to 50 % NaCl (99.9 %) and further ground for 12 h before washing additives with distilled water. Two leaching operations were performed to remove the additive. The final solid was then dried and calcined at a desired temperature. For the sake of brevity, the ground perovskite samples were designated as NP1-NP4 in Table-1.

TABLE-1
PREPARATION AND DESIGNATION OF $La(Co,Cu)O_3$ PEROVSKITES

	Sample	Calcination temp. (ºC)	S_{BET} (m^2/g)
CT1	$LaCoO_3$	600	2.1
CT2	$LaCo_{0.9}Cu_{0.1}O_3$	800	4.9
CT3	$LaCo_{0.8}Cu_{0.2}O_3$	800	6.2
CT4	$LaCo_{0.7}Cu_{0.3}O_3$	800	4.7
CT5	$LaCo_{0.6}Cu_{0.4}O_3$	800	5.8
CT6	$LaCo_{0.5}Cu_{0.5}O_3$	800	10.6
NP1	$LaCoO_3$	250	59.6
NP2	$LaCo_{0.9}Cu_{0.1}O_3$	250	17.5
NP3	$LaCo_{0.7}Cu_{0.3}O_3$	250	18.3
NP4	$LaCo_{0.5}Cu_{0.5}O_3$	250	12.1
NP5	$LaCo_{0.4}Cu_{0.6}O_3$	250	22.8

Catalyst characterizations: The specific surface area of all the obtained samples was determined by nitrogen adsorption at -196 ºC using OMNISORB 100. The chemical analyses of the perovskites and the residual impurities were performed by atomic absorption spectroscopy using a Perkin-Elmer 1100B spectrometer. Phase analysis and particle size determination were performed by X-ray powder diffraction (XRD) using a using a SIEMENS D5000 diffractometer with CuK_α radiation ($\lambda = 1.54059$ nm). Temperature-programmed reduction (TPR) experiments were carried out with a flow system operating on the RXM-100 connected with a quadrupole mass spectrometer (UTI 100) and a thermal conductivity detector (TCD). H_2-TPR was recorded by passing 5 vol. % of H_2/Ar (20 cm^3/min) from room temperature up to 800 ºC (10 ºC/min). SEM images were recorded on a JEOL JSM-840 with magnification of 25,000.

Catalytic activity: The catalytic tests were carried out in a stainless steel continuous fixed-bed flow micro-reactor (BTRS–Jr PC, Autoclave Engineers) at 68 atm (1000 psi), 4500 $L/kg_{cat}/h$. A mixture of syngas ($H_2/CO = 2/1$) was diluted in 15 vol. % helium. Butane was intercalated between the outlet-reactor and inlet-chromatography apparatus as an internal standard. 200 mg of catalyst was pretreated *in situ* with 15 vol. % of H_2/N_2 flow (20cm^3/min) prior to reaction test. The programmed temperature was ramped with 2 ºC/min and kept at 525 ºC for 6 h. Subsequently, reactor was cooled to the reaction temperature while pressure was increased to 68 atm by feeding the mixture of syngas. The reaction products were analyzed online by both a gas chromatography (GC-Varian CP-3800) using two capillary columns (Carboxen 1006 PLOT and CP-Sil 5 CB) equipped with TCD and FID detectors and mass chromatography (Varian Saturn 2200).

RESULTS AND DISCUSSION

Characteristics of perovskites: The main features of the perovskite samples in terms of surface area and particle size are given in Table-1. The conventional CT1-CT5 samples show relatively low surface areas. Phase analysis of XRD spectra (Fig. 1) indicated the presence of a single perovskite phase with the typical rhombohedral structure[10,13] up to x = 0.3. The d_{110}-spacing of such samples varies slightly with an increased amount of copper content, indicating the distortion of lattice structure as cobalt ions are replaced by copper (Table 2). At value of $x \geq 0.4$, the appearance of the reflections belonging

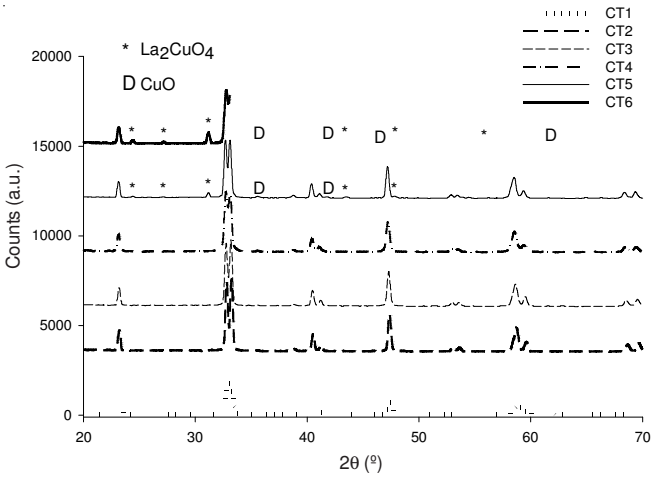

Fig. 1. XRD diffraction patterns of samples CT1-CT6

TABLE-2
PHYSICAL CHARACTERIZATIONS OF TWO $La(Co,Cu)O_3$ PEROVSKITE FAMILIES

Sample	$d_{(11\,0)}$ (Å)	2θ	Sizes (nm)	Crystalline phase[a]
CT1	2.719	32.91	48.0	P
CT2	2.721	32.72	46.3	P
CT3	2.728	32.73	42.8	P
CT4	2.729	32.79	42.8	P, La_2CuO_4
CT5	2.728	32.81	–	P, CuO, La_2CuO_4
CT6	2.727	32.69	–	P, La_2CuO_4, CuO
NP1	2.711	33.00	9.7	P
NP2	2.705	33.08	9.8	P
NP3	2.712	33.00	9.2	P
NP4	2.718	32.93	10.7	P, CuO
NP5	2.723	32.86	9.7	P, CuO, Co_3O_4

[a]P: Perovskite.

to La_2CuO_4 and CuO indicates the presence of small amount of these compounds in addition to $La(Co,Cu)O_3$ perovskite phase. The substitution of cobalt by copper in citrate-derived perovskite structure could only preserve up to x = 0.3.

On the contrary, Fig. 2 shows that no characteristic reflections of La_2CuO_4 could be detected with the NP2-NP4 samples prepared by grinding technique although a trace of CuO is detected at $x \approx 0.5$. XRD spectra of NP2-NP5 samples showed several singe peaks at $2\theta \approx 33.0, 40.6, 53.3$º. Moreover, full width at half maximum (FWHM) of the milled perovskites is more broaden than that of the conventional family. Therefore, it can be drawn the conclusion that the crystal domains of NP1-NP4 are smaller than those of CT1-CT4 samples[14,15]. Consequently, total surface area of NP1-NP-4 is expected to be higher than that of CT1-4 family as in good accordance with BET calculation (Table-2). The specific surface area of the CT1-CT6 perovskites is *ca.* 1-6 m^2/g.

Reducibility of perovskites: Transition metal ion can be usually extracted from perovskite lattice in the highly metallic phase as treated in hydrogen at a moderate temperature[3,7,9]. The temperature programmed reduction (H_2-TPR) of hydrogen was carried out from room temperature to 800 ºC in order to investigate the reducibility of two prepared perovskite families. Fig. 3 presents the H_2-TPR profiles of the conventional perovskite series.

Four CT1-CT4 samples display a double-step reduction of cobalt. The total reduction of Cu^{2+} to Cu^0 is expected to

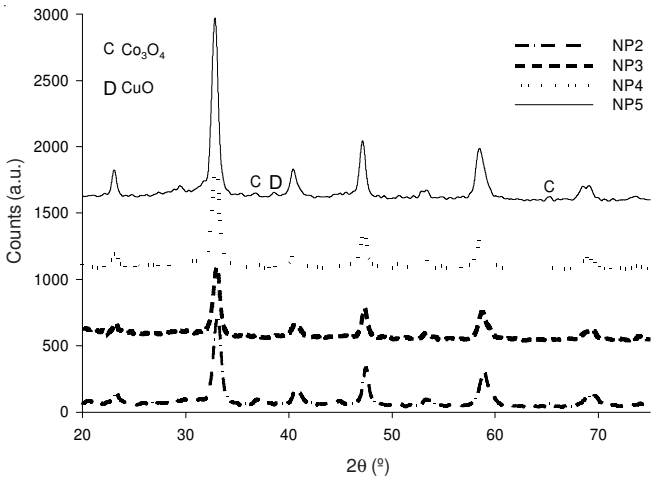

Fig. 2. XRD patterns of samples NP2-NP5

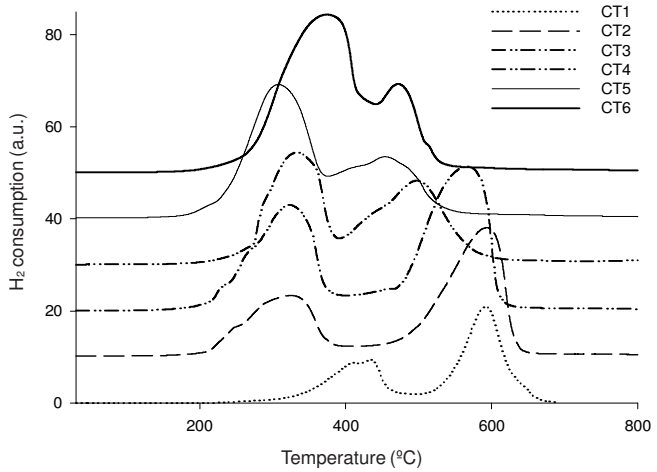

Fig. 3. Temperature-programmed reduction profiles of samples CT1-CT6

occur at a lower temperature peak[7,14,16]. Therefore, the first peak in the range of 180-390 ºC is attributed to reduction of Cu^{2+} and Co^{3+} to lower oxidation states with $x \leq 0.3$ and the second peak at 460-590 ºC is the complete reduction of Co^{2+} to metallic cobalt[10,16]. By increasing the copper substitution up to $0.3 < x \leq 0.4$, the maximum temperature of the first peak further decreases and the second peak appears a shoulder at 410-430 ºC, which is solely ascribed to the reduction of La_2CuO_4. In addition, the base line was not recovered after the first peak showing that the reduction the successive reduction step starts while the first peak is still in progress. At $x \leq 0.4$, the complete reduction of Co^{3+} to Co^{2+} and Cu^{2+} to Cu^0 occurs below 535 ºC and the superimposition of signals does not allow the determination of sequence of cobalt and copper reductions in $LaCoCuO_3$, CuO and La_2CuO_4. In contrast to the conventional perovskite samples, H_2-TPR diagrams of NP-family depicted in Fig. 4 display numerous visible peaks. The maximum temperature of the first peak is relatively higher than that of the corresponding citrate-derived perovskite, suggesting that the ground perovskites are likely more thermal stability under equivalent reducing conditions[14,17]. As mentioned above, the substitution of cobalt by copper also gives rise to the distortion of the cubic lattice and the formation of oxygen vacancies, various changes in distinct Co^{3+} environment[1,10,18]. Moreover,

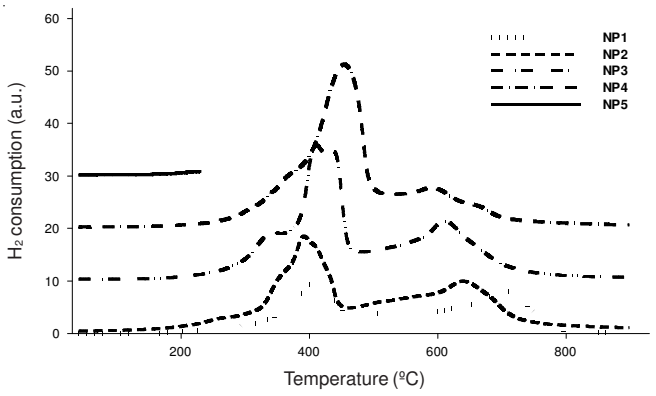

Fig. 4. Temperature-programmed reduction profiles of grinding perovskites

the grinding method was known to make nanoperovskites with particular morphology[14-16]. Indeed, SEM image of ground perovskite appears uniform particles with crystal domains on the order of 30-50 nm while that of conventional perovskite is present in a sponge-like network with the macropore diameter in the range of 3-6 mm. Consequently, coordination of ions in grain boundary of ground nanoparticles is assumedly different from that in the bulk (Fig. 5). Accordingly, copper and cobalt ions in grain boundaries are more easily reduced than those in the bulk, leading to appearance of some shoulders in the low temperature window.

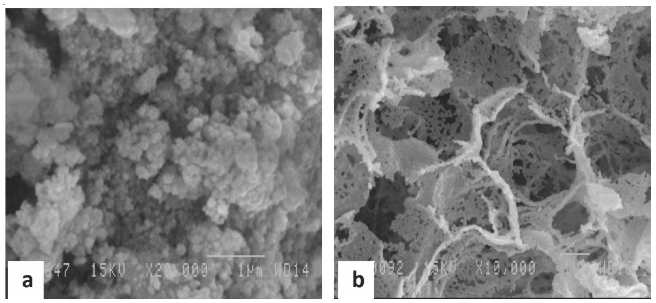

Fig. 5. SEM images of NP3 (a) and CT4 (b)

To elucidate this hypothesis, we have deconvoluted the H_2-temperature programmed reduction profiles of two representative samples in Fig. 6. It is clearly recognized that the low-reduction temperature peak is likely consisted of three deconvoluted peaks (Fig. 6a). The first one at 345 ºC is attributed to the conversion of Cu^{2+} to Cu^0, the higher peak at 410 ºC is described for the reduction of Co^{3+} on surface to Co^{2+} although the reduction of Cu^{2+} in the bulk happens at this temperature is not ruled[7,10,18]. The full reduction of Co^{3+}/Co^{2+} and Cu^{2+}/Cu^0 was almost obtained at 450 ºC (Fig. 6a). The mutual interaction between cobalt and copper sites in perovskite lattice leads to an increase in copper reduction temperature and diminution of the reduction temperature of cobalt ions[10,17,18]. Thus, the deconvoluted H_2-TPR profile for NP4 represents two peaks at lower temperature (Fig. 6b). The reduction of Co^{2+}/Co^0 in the copper-richer-perovskites also shifts remarkably to lower temperatures.

To confirm the formation of metallic metal at this temperature, we have collected XRD patterns for NP2 and NP4 samples at the reduction of 535 ºC. Under this condition, it is observed that the formation of intermediate phases, $LaCo(Cu)O_{3-x}$, La_2O_3, LaOOH and very weak reflection signals which are

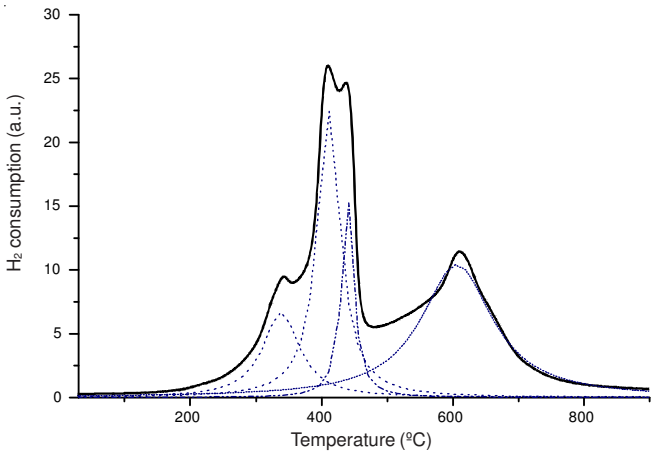

(a)

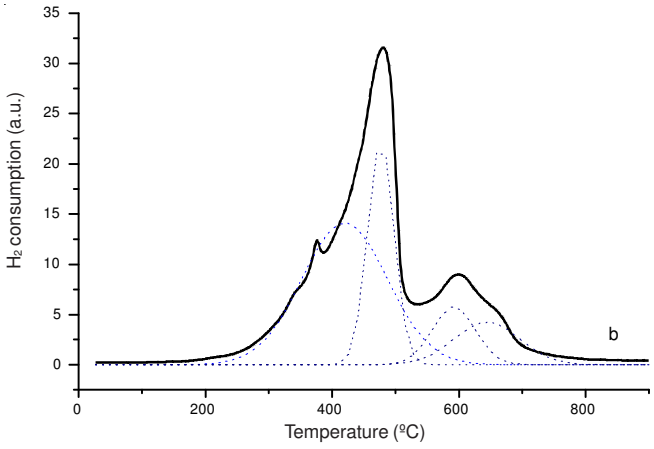

(b)

Fig. 6. Deconvolution profiles of H_2-TPR profile for NP2 (a), NP4 (b)

assigned to metallic copper and some cobalt in Fig. 7. This observation was explained by extracting of Co^0, Cu^0 in the initial perovskite lattice to produce dispersed metallic copper-cobalt. By increasing the cobalt substitution up to x = 0.5, the maximum temperature of the first peak further increases up to 485 ºC and the second gradually decreases to 590-610 ºC. A comparison between Figs. 3 and 4 shows that the reduction process of NP1-NP5 catalysts takes place at higher temperature, suggesting that they are better thermal stability[14,18].

Hydrogenation of carbon monoxide: A typical perovskite sample has been tested for syngas conversion showing that $LaCoCuO_3$ (x = 0 - 0.6) produced a homolog of hydrocarbons and linear primary alcohols, carbon dioxide[14,19]. The distribution

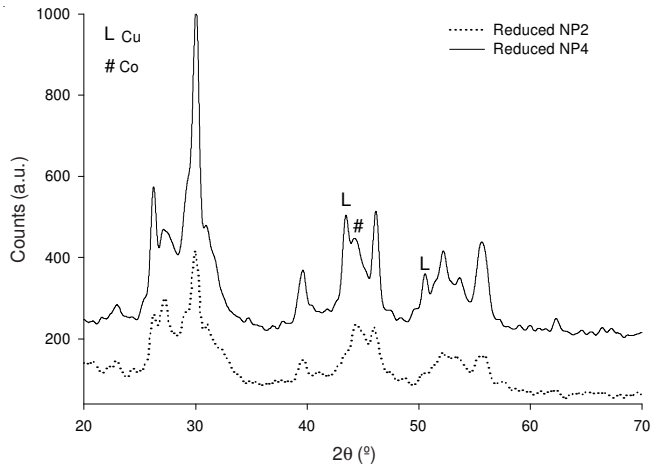

Fig. 7. XRD patterns of NP2 and NP4 reduced at 535 ºC

of products obtained in Table-3 indicates that the reaction is quite complex and can encompass the following reactions: Fischer-Tropsch reactions for hydrocarbons, alcohol synthesis, water-gas-shift reaction (WGS), *etc*. However, the total selectivity to alcohols takes values *ca.* 37-41 % with an exception of that obtained on some representative CT-samples. CO conversion over ground perovskites is much different from the value obtained on CT2-CT6 perovskites, but lower alcohol selectivity over conventional perovskite precursors is observed. This is associated with the difference in catalyst morphology (Fig. 5) and the dispersion of Co-Cu in the reduced form[16,19,20].

The ground perovskites have a higher surface area and better thermal stability that may preserve a better dispersion of Co-Cu metal under syngas exposure and reaction temperature. An existence in proximity of dual sites (Co and Co) facilitates the formation of carbon-chain-lengthened oxygenate products[14,18,20]. Thus, the alcohol selectivity is not only dependant on the catalyst composition, but also relates to the catalyst texture.

Alcohol selectivity is found to vary with the copper content[19]. The majority of methanol in alcohol product mixture is due to the favorable formation of methanol on copper sites[10,19-21]. Within hydrocarbons, methane is always a major product, but significantly suppresses with an increased copper content. For ground nanoperovskites, the selectivity to C_2^+-hydrocarbon varies from 30 to 41 % which is on a par with that to alcohols, implying the competition between alcohol and hydrocarbon formations on catalytic surface. For each perovskite series, it is quite difficult to compare the selectivity to product over

TABLE-3
CATALYTIC RESULTS IN SYNGAS CONVERSION INTO HYDROCARBONS AND ALCOHOLS[a]

Catalyst	Cu/Co ratio	Conv. (%)	Product selectivity (%, free-CO_2)							
			CH_4	C_{2+HC}	MeOH	EtOH	$C_{3+}OH$	ΣROH	α_{ROH}	α_{HC}
NP1	0	25.8	32.3	30.4	8.1	15.3	13.9	37.3	0.34	0.50
NP2	0.18	16.4	33.1	35.0	11.5	10.2	10.2	31.9	0.38	0.47
NP3	0.44	9.7	16.0	41.1	14.4	18.0	13.2	42.9	0.38	0.44
NP4	0.55	11.7	28.9	30.9	13.8	14.6	11.8	40.2	0.37	0.44
NP5	1.26	10.6	20.9	40.1	17.5	11.2	10.3	39.0	0.37	0.43
CT2	0.18	17.3	40.2	43.7	12.3	2.6	1.2	16.1	0.36	0.39
CT4	0.43	13.7	37.2	44.8	4.2	6.1	5.8	17.0	0.35	0.40
CT6	1.25	8.6	37.5	42.7	10.9	4.2	4.7	19.8	0.33	0.38

[a]Reaction conditions: 275 ºC; 4500 (L $kg_{cat.}^{-1}$ h^{-1}), (15 vol % He); H_2: CO = 2/1); 68 atm.

each sample since its test is unable to give a same conversion of CO at the reported conditions (Table-3). In this case, taking account of chain growth probability factors would provide more insight into catalytic behaviours. The growth factor of product carbon skeleton on each catalyst is calculated using Anderson-Schulz-Flory (ASF) distribution as described below[14,22]:

$$\ln X_n = n \ln \alpha + \ln \frac{1-\alpha}{\alpha}$$

where X_n is molar ratio of product, n the number of carbon atoms and α is the probability factor of the carbon skeleton[23-25]. In the present work, α values are from n = 1 (CH_3OH) to n = 7 (C_7OH) for α_{ROH} (alcohols) and from n = 2 to n = 11 for α_{HC} (hydrocarbons). A representative ASF plot for sample NP3 is drawn in Fig. 8.

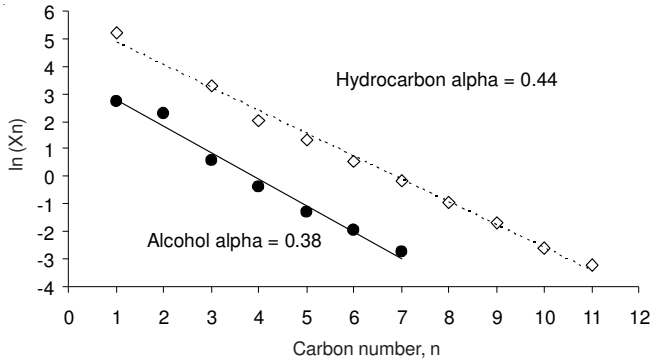

Fig. 8. ASF distributions of products at 275 ºC on sample NP3

The results indicate that the chain growth probability values of alcohols are relatively constant while those of hydrocarbons slightly vary with the changes in intra-lattice copper content[19]. This can be explained by the presence of Cu^{2+} in $LaCoO_3$ perovskite structure that diluted Co phase by alloying with copper (Fig. 7) after pretreatment with hydrogen[14,20,23]. The probability of chain growth of hydrocarbons (α_{HC}) is usually higher than that of alcohols (α_{ROH}) over perovskite catalysts; but α_{ROH} over ground perovskites is also better than the-one over citrate-derived samples. Thus the preparation route and catalyst morphology have significantly affected the formation of higher alcohols[14,19,20]. In the present study, the highest alcohol detected is heptanol (a trace of octanol) while undecane (in addition to a trace of dodecane) was found in the mixture of hydrocarbon products. The formation of a series of linear primary alcohols and normal paraffins in good agreement with an ASF distribution indicated that the mechanism likely takes place following insertion of C_1-intermediates such as methanol, CH_x moieties to propagate the carbon chains of products[23-25].

Conclusion

Two sets of $LaCo_{1-x}Cu_xO_3$ (x = 0-0.5) were prepared by different recipes. The milling synthesis allows the preparation of mixed $La(CoCu)O_3$ perovskites up to $x \approx 0.5$ and forms nanoperovskites while citrated complex method give only a maximal value of x = 0.5. Introduction of copper into perovskite lattice results in a distorted structure and strongly influences the reducibility of cobalt and the stability of all prepared perovskites. Under reducing conditions, the reduction of conventional perovskites CT1-CT6 passed through two steps whereas the ground samples NP1-NP4 occurred in a multiple-step. The reduction of cobalt promoted by copper neighbor takes place at lower temperature, which gives rise to the finely dispersed cobalt-copper on oxide-mixed matrix.

The reduced forms of perovskites were tested for the hydrogenation of syngas at high pressure. A homologue of hydrocarbons from methane to decane and a set of linear primary alcohols have been obtained. A mixture of hydrocarbon and alcohol products follows an ASF distribution. The reduced ground perovskite catalysts are rather active for alcohol synthesis while citrate-derived samples yield mainly hydrocarbons in addition of a small amount of oxygenated products. In both cases, an insertion of copper into $LaCoO_3$ perovskite lattice catalysts could suppress the formation of methane.

ACKNOWLEDGEMENTS

This research is funded by National Foundation for Science & Technology (Nafosted) through Project No. 104.99-2011.50.

REFERENCES

1. R. Lago, G. Bini, M.A. Pena and J.L.G. Fierro, *J. Catal*., **167**, 198 (1997).
2. N.A. Merino, B.P. Barbero, P. Grange and L.E. Cadus, *J. Catal*., **231**, 232 (2005).
3. Y.L. Gu, Y.X. Yang, Y.M. Qiu, K.P. Sun and X.L. Xu, *Asian J. Chem.*, **23**, 1247 (2011).
4. M.A. Pena and J.L.G. Fierro, *Chem. Rev*., **101**, 1981 (2001).
5. J.L.G. Fierro, *Catal. Today*, **8**, 153 (1990).
6. S. Aasland, H. Fjellvag and B.C. Hauback, *J. Solid State Chem*., **135**, 103 (1998).
7. P. Porta, S.D. Rossi, M. Faticanti, G. Minelli, I. Pettiti, L. Lisi and M. Turco, *J. Solid State Chem*., **146**, 291 (1999).
8. A. Baiker, P.E. Marti, P. Keusch, E. Fritsch and A. Reller, *J. Catal*., **146**, 268 (1994).
9. P. Ciambelli, S. Cimino, S.D. Rossi, M. Facticanti, L. Lisi, G. Minnelli, I. Pettiti, P. Porta, G. Russo and M. Turco, *Appl. Catal. B*, **24**, 243 (2000).
10. L. Lisi, G. Bagnasco, P. Ciambelli, S.D. Rossi, P. Porta, G. Russo and M. Turco, *J. Solid State Chem*., **146**, 176 (1999).
11. H. Provendier, C. Petit and A. Kiennemann, *Surf. Chem. Catal*., **4**, 57 (2001).
12. J.O. Petunchi, J.L. Nicastro and E.A. Lombardo, *J. Chem. Soc. Chem. Commun*., 467 (1980).
13. A.W. Webb, E.F. Skelton, S.B. Qadri and E.R. Carpenter, *J. Solid State Chem*., **102**, 519 (1993).
14. N. Tien-Thao, M.H. Zahedi-Niaki, H. Alamdari and S. Kaliaguine, *J. Catal*., **245**, 348 (2007).
15. Q. Zhang, J. Lu and F. Saito, *Powder Technol*., **122**, 145 (2002).
16. N. Tien-Thao, M.H. Zahedi-Niaki, H. Alamdari and S. Kaliaguine, *J. Solid State Chem*., **181**, 2006 (2008).
17. R. Zhang, A. Villanueva, H. Alamdari and S. Kaliaguine, *J. Mol. Catal. A*, **258**, 22 (2006).
18. L. Huang, M. Bassir and S. Kaliaguine, *Appl. Surf. Sci*., **243**, 360 (2005).
19. J.A.B. Bourzutschky, N. Homs and A.T. Bell, *J. Catal*., **124**, 52 (1990).
20. X. Xiaoding, J.J.F. Scholten and D. Mausbeck, *Appl. Catal. A*, **82**, 91 (1992).
21. M. Xu, M.J.L. Gines, A.-M. Hilmen, B.L. Stephens and E. Iglesia, *J. Catal*., **171**, 130 (1997).
22. R.B. Anderson, The Fischer-Tropsch Synthesis, Academic Press, Inc. (1983).
23. D.J. Elliott, *J. Catal*., **111**, 445 (1988).
24. M. Xu, M.J.L. Gines, A.-M. Hilmen, B.L. Stephens and E. Iglesia, *J. Catal*., **171**, 130 (1997).
25. M.R. Morrill, N.T. Thao, H. Shou, D.J. Barton, D. Ferrari, R.J. Davis, P.K. Agrawal and C.W. Jones, *Catal. Lett*., **142**, 875 (2012).